24th COBEM - 2017

24th ABCM International Congress of Mechanical Engineering
December 3-8, 2017, Curitiba, PR, Brazil

COBEM-2017-1395
STUDIES ON AEROELASTIC OPTIMIZATION OF COMPOSITE SWEPT WINGS

Hermann Luís Lebkuchen
lebkuchen@ita.br
Roberto Gil Annes da Silva
gil@ita.br
Technological Institute of Aeronautics, ITA. Praça Marechal Eduardo Gomes, 50 - Vila das Acacias, São José dos Campos - SP, Brazil
Carlos Eduardo de Souza
Federal University of Santa Maria, UFSM. Av. Roraima, 1000 - Camobi, Santa Maria - RS, Brazil
carlos.souza@ufsm.br

Abstract. *In an effort to explore structural challenges justified by aerodynamic advantages of swept wings, this paper presents the effects of sweep angle in aeroelastic stability response of a simplified wing model with a ballast mass attached on its tip. The aeroelastic response of wing models made of aluminum as well as carbon fiber-epoxy resin composite are investigated. First, the influence of ballast mass position on flutter and divergence speeds is presented for the three swept aluminum wings. The flutter speed results calculated with the numeric model are validated experimentally with wind tunnel tests. Proposed lay-ups made of constant stiffness composite have their aeroelastic response mapped over a defined fiber orientation domain. These composite wings are aeroelastic tailored to maximize flutter speeds for unswept, forward and backward swept models. The optimization is performed with a numeric aeroelastic stability objective function that relates flutter and divergence speeds as a function of lay-up orientation. The aeroelastic stability function couples structural finite element model with aerodynamic panel model. The aeroelastic system is solved using the G-method for subsonic unsteady incremental aerodynamics. Proposed lay-ups are optimized to maximum flutter speeds using genetic algorithm method. The management of aeroelastic stability and tailoring solutions is automated with the development of in house software. It is presented that the optimized lay-ups for forward swept wings can not only overcome the undesired effect of static aeroelastic divergence without losing the aerodynamic benefits but also result in a lighter structure.*

Keywords: *aeroelastic tailoring, swept wing, fiber reinforced composite materials, optimization, aeroelasticity.*

1. INTRODUCTION

The effects of sweep angle on aeroelastic stability of a simplified flexible wing model is the focus of the present work. The motivation for current research lays on the aerodynamic advantages of forward swept wings (FSW) and backward swept wings (BSW) in relation to unswept wings (USW), as presented in literature by Whitford (1987); Krüger *et al.* (2014); Krone (1980). Besides the aerodynamic advantages, the structural challenges related with the design of FSW configuration represent an interesting field for aeroelastic tailoring techniques when designing structures made of fiber reinforced composites with constant and variable stiffness.

Even presenting better aerodynamic characteristics, as reported by Bisplinghoff *et al.* (2002) and Krone (1975) , the FSW has been ruled out in traditional aircraft mainframe designs because of high structural weight necessary to handle severe loadings in wing root caused by the static aeroelastic divergence phenomenon (Försching, 2013). In aerodynamic perspective, the leading edge of FSW configuration is more orthogonal to the free stream flow. Thus, crossflow instabilities at the leading edge and turbulent boundary layer are decreased (Uranga *et al.*, 2011). Redeker and Wichmann (1991) reported that crossflow instabilities lead to a longer chordwise laminar flow, which reduces the friction drag and increases lift-drag ratio. This behavior induces the stall to start inboard close to the fuselage, resulting in great static lateral as well as longitudinal and directional stability. The FSW combined with canards may make FSW spinning-proof, according to Whitford (1987). Besides that, as the flow is directed inboard in FSW, it increases the aileron effectiveness being possible to design smaller control surfaces. In the aircraft tail, the inboard flow makes possible to design smaller horizontal stabilizer and elevator. On the other hand, for BSW the flow is directed outboard. Hence, the stall starts outboard in wing tip, decreasing the aileron effectiveness and unleashing tip vortices (Gudmundsson, 2013).

The wings with forward sweep angle are interesting not only because of aerodynamic purposes, but represent also a challenge for structural design due static aeroelasticity. The FSW configuration induces the torsion-divergence statical aeroelastic phenomenon.The torsion up is coupled with pitch up resulting in the wash in behavior, so the local tip attack

angle is increased becoming higher than the root attack angle. This behavior couples positive bending and torsion components since the structure is flexible, unleashing divergence phenomenon. Thus, a stiffer structure needs to be designed for FSW in order to guarantee structural integrity (Piening, 1984; Försching, 2013) .

The first effort to investigate the influence of forward sweep angle on aircraft design considering aeroelastic effects was published by Diederich and Budiansky (1948) via a theoretical determination of the most fundamental aeroelastic parameters. Following that, Diederich and Foss (1953) presented charts and approximation formulas to estimate the FSW effects on divergence speed, spanwise lift distribution, rolling moment coefficient and roll rate due to the deflection of ailerons at subsonic and supersonic speeds. However, due the fact that at that time only isotropic metallic materials such as aluminum were used in aeronautical structure design, the FSW configuration was not further considered due the high structural weight necessary to provide the stiffness to overcome torsion divergence. Further, Waddoups *et al.* (1971) presented the first application of anisotropic mechanical properties of fiber reinforced composite materials to enhance the aeroelastic response of a wing. Following that, Krone (1975) adopted the anisotropic mechanical properties in FSW made of composite materials to overcome torsion divergence phenomenon, what brought back the feasibility of such configuration in aeronautic design. Both authors, Waddoups *et al.* (1971) and Krone (1975), adopted the design methods based on the mechanics of composites published by Tsai (1966). Hence, Krone (1975) concluded that by properly tailoring composite laminates, the structural weight penalty associated with the divergence could be greatly reduced.

Following those initial contributions, the FSW concept was further investigated by Weisshaar (1978, 1979, 1980, 1981); Ricketts and Doggett Jr (1980); Hertz and Picchioni (1981); Piening (1984), among others. Based on the knowledge formulated by these authors, Redeker and Wichmann (1991) published a judicious aerodynamic analysis comparing BSW and FSW potential to achieve laminar flow wings. The authors concluded that FSW comprehends in a favorable concept for laminar flow wings, stating that a more stable laminar boundary layer is created due crossflow instability and attachment line transition.

Since the theoretical interpretation about aerodynamics and structural behavior of wings with negative sweep angle has been well described in literature, it has been proved that the divergence may be overcome by correctly disposing fiber orientation on laminate fiber reinforced composites. Regarding that, negative swept wings represent an interesting non conventional design either for military or civilian aircraft design. Thus, the ability to design the most appropriate laminate stack sequence which gives the lower structural weight and wing root loading while giving higher divergence and flutter speed is a major requisite to design such airframe. As presented by Weisshaar (1995), this optimization approach is referred as *"aeroelastic tailoring"* or *"aeroelastic passive control"*. This technique aims mostly to minimize the structure mass or wing root bending while maximizing divergence speed, buckling factor, aileron effectiveness, flutter speed, among others. The optimization variables may be either discrete through fiber angle and lamina thickness, as performed by Stanford and Jutte (2014); Roldo (2016); Tian *et al.* (2016), or continuous through lamination parameters as the following references present Dillinger *et al.* (2013); Werter *et al.* (2016); Thuwis *et al.* (2010); Kameyama and Fukunaga (2007); Liu *et al.* (2015).

This work deals with a simplified flexible wing model made of aluminum and constant stiffness carbon fiber-epoxy reinforced composite material, similar to the one presented by Jaworski (2009). Three different sweep angles are defined for aluminum and composite wings: USW with $\Lambda = 0°$; FSW or negative sweep with $\Lambda = -15°$; and BSW or positive sweep with $\Lambda = +15°$. The three models have tip and root chord parallel to flow stream, following the recommendations proposed by Krone (1975). A ballast mass is attached to tip chord in order to couple second bending and first torsion structural vibrational modes. The ballast mass position is varied along the chord tip and its influence in aeroelastic stability is presented for aluminum models. These results are validated with wind tunnel tests performed at Technological Institute of Aeronautics. In order to tailor this flexible structure for aeroelastic response, the orientation of fibers in carbon fiber-epoxy wings are firstly mapped over a defined domain and then optimized using Matlab® genetic algorithm tool. The aeroelastic stability function is implemented in Matlab® by coupling the structural model based on finite elements implemented with commercial software DS Abaqus® and unsteady incremental aerodynamic model based on panel method implemented with commercial software Zaero® . The aeroelastic evolution as well as flutter and divergence speed are calculated with the G-method ZONA6 available in Zaero® for subsonic unsteady aerodynamics. The management of models, aeroelastic response and tailoring is automated with the development of an in-house software entitled ASA-T.

2. AEROELASTIC SYSTEM

The aeroelastic system consist of a structural and aerodynamic model. The structure is discretized with finite element technique using the software DS Abaqus® . The aerodynamic model is modeled with panel method using the software Zaero® . The aeroelastic stability solution is performed with the G-Method ZONA6 for subsonic unsteady incremental aerodynamics. Next, the fiber reinforced composite lay-up is mapped and optimized using the Matlab® genetic algorithm toolbox. Both structural and aerodynamic models are automated with an in-house tool developed in Matlab® . The tool is entitled ASA-T (Aeroelastic Stability Analysis Tool). When the optimization is coupled with aeroelastic stability analysis, the tool is called OPTASA-T. The methodology implemented is presented in the flowchart depicted in Fig. 1.

The mathematical model is presented from now based on Bisplinghoff *et al.* (2002); Försching (2013); Fung (2002)

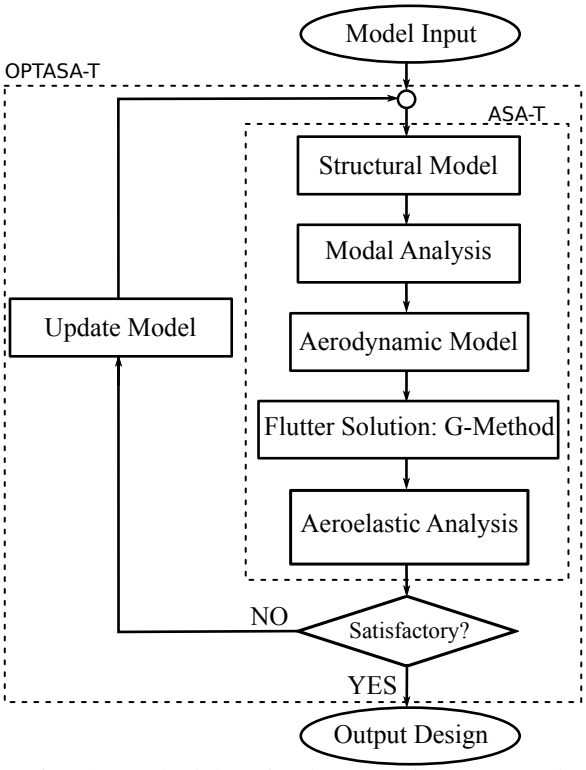

Figure 1: Flowchart representing the methodology implemented in ASA-T and OPTASA-T with Matlab® .

and ZONA-Technology (2009); Balvedi Junior (2010). The equation of motion (EOM) for a general dynamic system without damping and considering only incremental unsteady aerodynamic loadings as external force is written as:

$$[\mathbf{M}]\{\ddot{\mathbf{x}}(t)\} + [\mathbf{K}]\{\mathbf{x}(t)\} = \{\mathbf{P}\} = \{\mathbf{F_a}\}. \tag{1}$$

The finite elements and panels defined in structural and aerodynamic models, respectively, need to be related in order to transfer the aerodynamic loads to the structure. Thus, the right loading term in Eq. 1 is defined as:

$$\{\mathbf{F_a}\} = [\mathbf{G_s}]^T\{\mathbf{f_a}(t, \{\dot{\mathbf{x}}\}, \{\mathbf{x}\})\}, \tag{2}$$

where $[\mathbf{G_s}]$ is the displacement interpolation matrix from structure to aerodynamic degrees of freedom (DGOF) calculated with splines (Harder and Desmarais, 1972). The incremental unsteady aerodynamic loading $\{\mathbf{f_a}(t, \{\dot{\mathbf{x}}\}, \{\mathbf{x}\})\}$ is now written as a function of time, displacement and velocity. Considering the hypothesis of linear system and small displacements, the EOM 1 is decoupled with generalized coordinates $\{\mathbf{q}(t)\}$. Thus:

$$\{\mathbf{x}\} = [\phi]\{\mathbf{q}(t)\}, \tag{3}$$

where $[\phi]$ is the eigenvectors matrix.

Rewriting the EOM given in 1 with generalized coordinates presented in Eq. 3, it results into:

$$[\bar{\mathbf{M}}]\{\ddot{\mathbf{q}}(t)\} + [\bar{\mathbf{K}}]\{\mathbf{q}(t)\} = [\phi]^T\{\mathbf{F_a}\}, \tag{4}$$

where $[\bar{\mathbf{M}}] = [\phi]^T[\mathbf{M}][\phi]$ and $[\bar{\mathbf{K}}] = [\phi]^T[\mathbf{K}][\phi]$ are the generalized mass and stiffness matrices, respectively. The right term representing the unsteady incremental aerodynamic loads is obtained with the panel method employed in ZONA6, introduced in Subsec. 2.1 The mass $[\mathbf{M}]$ and stiffness $[\mathbf{K}]$ matrices are calculated with the finite element model and presented in Subsec. 2.2

2.1 Aerodynamic Model

The term $\{\mathbf{f_a}(t, \{\dot{\mathbf{x}}\}, \{\mathbf{x}\})\}$ is written in Eq. 2 multiplied by splines interpolation matrix. Hence, the incremental unsteady aerodynamic loading is defined as:

$$\{\mathbf{f_a}(t, \{\dot{\mathbf{x}}\}, \{\mathbf{x}\})\} = q_\infty[\mathbf{AIC}(Ma, k)]\{\mathbf{x_a}\}, \tag{5}$$

where $[\mathbf{AIC}(Ma, k)]$ is the aerodynamic influence coefficient matrix. The $[\mathbf{AIC}]$ is a function of the Mach number $Ma = V_\infty / V_{sound}$ and reduced frequency:

$$k = \frac{\boldsymbol{\omega}\, c_{ref}}{V_\infty}. \tag{6}$$

The term $\boldsymbol{\omega}$ is the structure natural frequency in $[rad/s]$, c_{ref} is the reference chord, and $V_{\infty,min}$ the true flow stream velocity. Replacing Eq. 5 in the right term of EOM 4, it becomes:

$$\{\bar{\mathbf{F}}_\mathbf{a}\} = q_\infty [\boldsymbol{\phi}]^T [\mathbf{G_s}]^T [\mathbf{AIC}(Ma, k)] \{\mathbf{x_a}\}. \tag{7}$$

Following the same logic presented above and rewriting the aerodynamic DGOF with generalized coordinates, it leads to: $\{\mathbf{x_a}\} = [\boldsymbol{\phi_A}]\{\boldsymbol{\eta}\} = [\mathbf{G_s}][\boldsymbol{\phi}]\{\boldsymbol{\eta}\}$. Rewriting Eq. 7 with generalized coordinates, it reads:

$$\{\bar{\mathbf{F}}_\mathbf{a}\} = q_\infty [\boldsymbol{\phi}]^T [\mathbf{G_s}]^T [\mathbf{AIC}(Ma, k)][\mathbf{G_s}][\boldsymbol{\phi}]\{\boldsymbol{\eta}\}. \tag{8}$$

In ZONA-Technology (2009), the generalized aerodynamic influence coefficient matrix $[\mathbf{Q}_A(i, k)]$ reads:

$$[\mathbf{Q}_A(i, k)] = [\boldsymbol{\phi}]^T [\mathbf{G_s}]^T [\mathbf{AIC}(Ma, k)][\mathbf{G_s}][\boldsymbol{\phi}]. \tag{9}$$

Thus, $\{\bar{\mathbf{F}}_\mathbf{a}\} = q_\infty [\mathbf{Q}_A(i, k)]\{\boldsymbol{\eta}\}$. Replacing this relation in EOM 4, it results into:

$$[\bar{\mathbf{M}}]\{\ddot{\mathbf{q}}(t)\} + [\bar{\mathbf{K}}]\{\mathbf{q}(t)\} = q_\infty [\mathbf{Q}_A(i, k)]\{\boldsymbol{\eta}\}. \tag{10}$$

Finally, the EOM 10 is transformed to frequency domain since flutter comprehends in a stability problem. Hence, the resultant EOM to flutter solution in frequency domain is given by the following eigenproblem when considering $\{\mathbf{q}(t)\} = \sin(\omega t)$ in Eq. 10:

$$\left[\omega^2 [\bar{\mathbf{M}}] + [\bar{\mathbf{K}}] - q_\infty [\mathbf{Q}_A(i, k)]\right] \{\boldsymbol{\eta}\} = \{\mathbf{0}\}. \tag{11}$$

The solution of Eq. 11 solves the flutter dynamic stability aeroelastic problem. The flow speed is varied in dynamic pressure term by user input discrete values in Zaero®. For each discrete dynamic pressure value the frequency and damping factor are determined. The combination of these results ables to represent the VGF (velocity - damping - frequency) diagram. The ASA-T automatically creates Zaero® cards for flutter solution based on the model input options. Besides that, ASA-T automatically reads VGF diagrams identifying not only flutter and divergence speeds but also which vibration modes get coupled.

2.2 Structural Model

The structure model is implemented with the finite element method (FEM) using the software DS Abaqus®. The rectangular 2D four-node linear shell S4R element is used. The S4R is a general purpose element which allows transverse shear deformation (Reddy, 2005), it is adequate for small membrane strains and arbitrary large rotations cases. The shear and locking problems are avoided by the reduced integration, what guarantees the element robustness. The displacement vector is composed by the following DGOF: $\{\mathbf{x}\}^T = \begin{bmatrix}\mathbf{u_1} & \mathbf{u_2} & \mathbf{u_3} & \boldsymbol{\theta_1} & \boldsymbol{\theta_2}\end{bmatrix}$, where $\mathbf{u_i}$ are the nodal displacements and $\boldsymbol{\theta_i}$ are the nodal rotations. As presented in aerodynamic model, in order to solve the flutter problem it is necessary to perform a modal analysis to obtain the structure eigenvectors and eigenvalues. Thus, the EOM 4 is rewritten for free vibration considering the generalized coordinates as a periodic function $\{q_i(t)\} = \eta_i \sin(\omega_i t)$, as:

$$([\mathbf{K}] - \{\boldsymbol{\lambda}\}[\mathbf{M}])\,[\boldsymbol{\phi}] = \{\mathbf{0}\}. \tag{12}$$

The modal analysis is performed and the eigenvalues $\{\boldsymbol{\lambda}\} = \{\boldsymbol{\omega}\}^2$ and eigenvectors $[\boldsymbol{\phi}]$ are calculated with the *lanczos* eigenvalue solution technique (Lanczos, 1950).

The structure stiffness and mass matrices are necessary to calculate natural frequencies and modal shapes. The matrices for isotropic structure made of aluminum follow the well known method described in Reddy (2005). The derivation of mass and stiffness for composite shell structure is briefly presented below, following Reddy (2004). Thus, the distributed forces $[\mathbf{N}]$ and moments $[\mathbf{M}]$ are given by:

$$\begin{bmatrix}\{\mathbf{N}\} \\ \{\mathbf{M}\}\end{bmatrix} = \begin{bmatrix}[\mathbf{A}] & [\mathbf{B}] \\ [\mathbf{B}] & [\mathbf{D}]\end{bmatrix} \begin{Bmatrix}\{\boldsymbol{\epsilon}\} \\ \{\boldsymbol{\kappa}\}\end{Bmatrix}, \tag{13}$$

where $\{\boldsymbol{\epsilon}\}$ are the in-plane strains and $\{\boldsymbol{\kappa}\}$ the curvatures (Daniel *et al.*, 2006). The laminate stiffness matrices $[\mathbf{A}]$, $[\mathbf{B}]$ and $[\mathbf{D}]$ read, respectively:

$$[\mathbf{A}] = \sum_{k=1}^{n} [\bar{\mathbf{Q}}]^k (t_k - t_{k-1}), \tag{14}$$

$$[\mathbf{B}] = \frac{1}{2}\sum_{k=1}^{n}[\bar{\mathbf{Q}}]^k(t_k^2 - t_{k-1}^2), \tag{15}$$

$$[\mathbf{D}] = \frac{1}{3}\sum_{k=1}^{n}[\bar{\mathbf{Q}}]^k(t_k^3 - t_{k-1}^3). \tag{16}$$

The finite element stiffness matrix $[\mathbf{K}]$ rewritten in terms of laminate stiffness matrices is calculated by the following expression:

$$[\mathbf{K}_{FEM}] = \int_{-1}^{+1}\int_{-1}^{+1}\left[[\mathbf{F}_1]^T[\mathbf{A}][\mathbf{F}_1] + [\mathbf{F}_1]^T[\mathbf{B}][\mathbf{F}_2] + [\mathbf{F}_2]^T[\mathbf{B}][\mathbf{F}_1] + [\mathbf{F}_2]^T[\mathbf{D}][\mathbf{F}_2]\right]|[\mathbf{J}]|d\eta d\xi. \tag{17}$$

The lumped mass matrix reads:

$$[\mathbf{M}_{FEM}] = \int_{\Omega_{FEM}}[\mathbf{N}]^T\{\boldsymbol{\gamma}\}[\boldsymbol{N}]d\Omega_{FEM}. \tag{18}$$

The ASA-T automatically creates an input finite element model file with extension `.inp` for DS Abaqus® through the shell general stiffness element. Thus, the matrices $[\mathbf{A}]$, $[\mathbf{B}]$ and $[\mathbf{D}]$ are calculated with ASA-T. Besides that, ASA-T runs the modal analysis and reads the total mass of model as well as the desired number of structure eigenvalues and eigenvectors, which are used to solve the eigenproblem in Eq. 11 with Zaero®.

2.3 Optimization Problem

The aeroelastic tailoring strategy adopted in this work is defined as a multiple constrained problem, as follows:

$$\begin{aligned} &\max_{(\theta)_k} V_f((\theta)_k) \\ &\text{s.t.: } g_i = \qquad \Delta(\theta)_k \leq \theta_{lim} \end{aligned} \tag{19}$$

The optimization method employed to search the best lay-up orientation is the genetic algorithm (GA). The GA is performed with the Matlab® optimization toolbox (Inc., 2017). The OPTASA-T automatically calls the GA toolbox and links it with the aeroelastic stability function.

3. RESULTS

3.1 Isotropic Flexible Wing

In order to validate the aeroelastic stability function implemented in ASA-T, the aeroelastic model of an isotropic flexible wing made of aluminum 2024T3 clad, similar to that used in Jaworski (2009), is modeled. Three different sweep angles are defined: USW with $\Lambda = 0°$; FSW with $\Lambda = -15°$; and BSW with $\Lambda = +15°$. A ballast mass is attached to wing tip and its position is varied chordwise to investigate flutter and divergence behavior. The numerical flutter speeds are validated with experimental wind tunnel tests performed at Laboratory Prof. Feng in Technological Institute of Aeronautics. The geometry, mechanical properties and simulated flight conditions are listed in Tab. 1. The aluminum mechanical properties are experimentally determined with a mechanical tensile test and video gauge sensors at the Lightweight Structures Laboratory in the Institute of Technological Research (LEL/IPT).

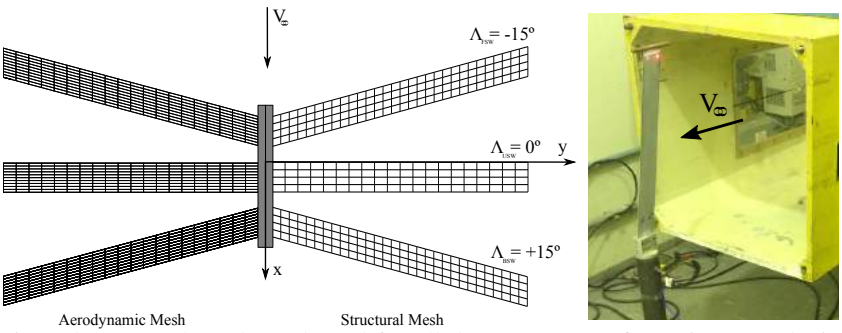

Figure 2: Aerodynamic and structural meshes adopted for all three swept configurations are depicted in left. The right figure depicts the FSW in wind tunnel test.

The aerodynamic as well as structural meshes defined in the numerical implementation are depicted in Fig. 2 left and right, respectively, for USW, FSW, and BSW configurations. Both meshes discretization are defined after convergence analysis of natural frequencies for FEM and flutter speed for panel method. The Fig. 2 left, depicts the wind tunnel test of FSW model, however, all three swept configurations were experimentally investigated. For USW one aluminum model was manufactured, while FSW and BSW comprehends the same model, which is rotated in $180°$ in relation to y axis.

Table 1: Values adopted for isotropic aluminum 2024 T3 clad; flexible wing geometry; ballast mass inertias; and flight condition.

Property	Symbol	Value	Unit
Elasticity Modulus	E_{Al}	68.20	GPa
Poisson's Ratio	ν_{Al}	0.33	-
Density	ρ_{Al}	2800	kg/m^3
Wing Half Span	$b/2$	0.33	m
Wing Chord	$c_{tip} = c_{root}$	0.04	m
Thickness	t	$8.124\ 10^{-4}$	m
Ballast Mass	m_b	0.03458	kg
Inertia Moment x-x	$I_{xx,b}$	0	$kg\,m^2$
Inertia Moment y-y	$I_{yy,b}$	$1.858\ 10^{-5}$	$kg\,m^2$
Inertia Moment z-z	$I_{zz,b}$	$1.858\ 10^{-5}$	$kg\,m^2$
Flight Altitude	h	0	m
Air Density	ρ_{air}	1.225	kg/m^3
Flow Velocity Range	V_∞	$[0 \dots 70]$	m/s

Since the structure is made of aluminum no tailoring related with stiffness properties is performed in this case. However, the position of ballast mass is varied chordwise from $x/c = 0$ up to $x/c = 1.0$, in relation to the wing leading edge with 0.125 increments, changing the inertia properties and consequently the aeroelastic stability. Thus, regarding the flowchart of Fig. 1, the aeroelastic stability of USW, FSW and BSW models modeled with properties given in Tab. 1 is performed. The flutter as well as divergence speeds are depicted in Fig. 3 as function of ballast mass position in terms of x/c ratio.

In Fig. 3a, the flutter speeds for all swept models are superposed in the same graph, it results of thirty VGF solutions performed with ASA-T. The experimental values obtained in wind tunnel tests are presented by hexagon markers of same color of respective numeric cases. Only cases up to $33m/s$ could be experimentally investigated because of wind tunnel maximum speed limitation. According to Fig. 3a, the flutter speed behavior is horizontally shifted in relation to x/c depending on the swept configuration. The BSW, which shifts the wing elastic line backwards, has flutter speeds below $33m/s$ when the ballast mass is positioned at $x/c = 0.000$ and $xc = 0.125$. Besides that, USW has four flutter speeds below $33m/s$ and FSW eight cases. This behavior is explained based on the structural modes of elastic structure, second bending and first torsion, which are coupled when flutter occurs. Since the elastic line is shifted forward in FSW case, the mode coupling may be reached with lower aerodynamic loads. The contrary is valid for BSW, since the wing elastic line is shifted backward in relation to USW case. The experimental results are in good agreement with numeric values.

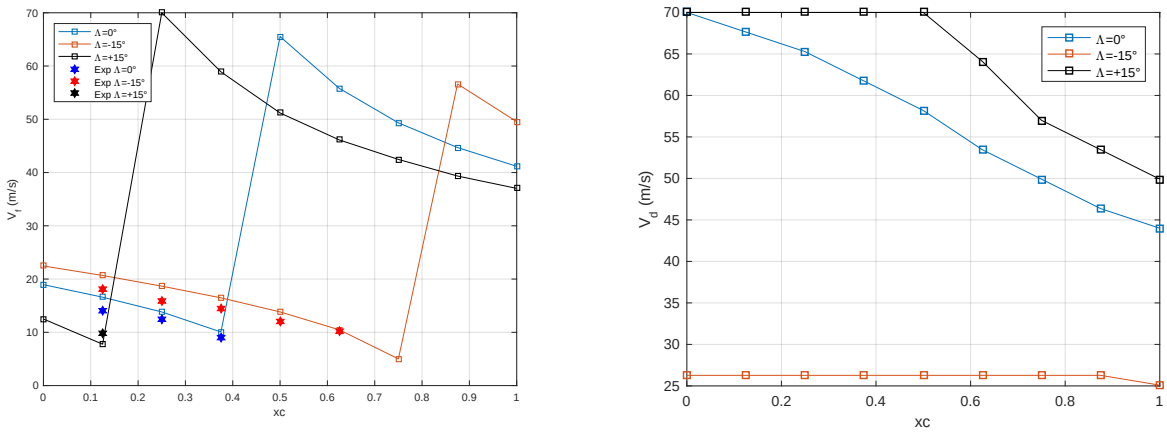

(a) Flutter speed versus x/c ballast mass position. (b) Divergence speed versus x/c ballast mass position.

Figure 3: Results of flutter and divergence speeds for USW, FSW and BSW models according to ballast mass x/c position.

In Fig. 3b the divergence speed for each swept case is plotted in relation to x/c ballast mass position. As presented in the literature, the FSW has lower divergence speeds in relation to other models because of wash in effect, which leads the structure to high deflections due the bending-torsion coupling. If a value of divergence speed at least equal to the USW model wants to be reached for FSW with ballast mass at $x/c = 0.625$, for instance, the structure thickness should be increased in 70%, what results in a weight increase from $m_{FSW,t_0} = 65.7g$ to $m_{FSW,t_d} = 87.4g$, or 33%. This proves the weight drawback issue when designing FSW made of isotropic materials such as aluminum.

3.2 Constant Stiffness Composite Flexible Wing

The aeroelastic stability of a constant stiffness fiber reinforced composite wing with same geometry properties as presented for isotropic case in Tab. 1 is performed. The fiber orientation angle is defined equal zero when the fiber is parallel to the chord, and equal $90°$ when fiber is parallel to wing span in USW case. The investigation is divided in two parts, firstly the fiber orientation angle is varied in domain $-90° \leq \theta_{i,j} \leq +90°$ with $5°$ step in order to map the flutter and divergence stabilities for a group of laminates. Following that, the GA optimization method is coupled with ASA-T to aeroelastic tailor the proposed model to maximum flutter speeds. The lay-up respects the following nomenclature in this work: $[\theta_{i,j}]$, where $_i$ address the index number and $_j$ the number of plies associated with each index. Other nomenclature particularities follow the definitions given in Daniel *et al.* (2006). The mechanical properties of carbon fiber-epoxy resin AS4/3501-6 fiber reinforced composite are presented in Tab. 2 based on reference Shokrieh and Lessard (2000).

Table 2: Mechanical properties of carbon fiber-epoxy resin AS4/3501-6 composite (Shokrieh and Lessard, 2000).

Property	Symbol	Value	Unit
Elasticity Modulus in xx	E_{xx}	147	GPa
Elasticity Modulus in yy and zz	$E_{yy} = E_{zz}$	9.00	GPa
Elasticity Modulus in xy and xz	$E_{xy} = E_{xz}$	5.00	GPa
Elasticity Modulus in yx	E_{yx}	3.00	GPa
Poisson in xy and xz	$\nu_{xy} = \nu_{xz}$	0.30	-
Poisson in yz	ν_{yz}	0.42	-
Ply Thickness	t_{ply}	0.16	mm
Density	ρ_c	1560	kg/m^3
Fiber limit angle	θ_{lim}	± 90	$°$

The following lay-ups are investigated in this work: (I) $[\theta_{1,1}]_S$, symmetric with two plies equally orientated; (II) $[\theta_{1,1}\ \theta_{2,1}]$, asymmetric with two plies. All cases presented in constant stiffness composite have the ballast mass, whose inertia properties are defined in Sec. 3.1 attached at $x/c = 0.375$ position. Each laminate is mapped with $5°$ step in fiber orientation angle. Thus, lay-up (I) has one variable in $\theta_{1,j}$, resuming the analysis in 37 VGF diagram solutions for each sweep configuration, what means 111 solutions for each lay-up. Moreover, the lay-up (II) has two fiber orientation variables in $\theta_{1,j}$ and $\theta_{2,j}$. It results in 1369 VGF diagram solutions for each sweep configuration, that are 4107 solutions. Thus a total of 4216 runs are performed in the mapping phase. The solution of aeroelastic stability is presented in Fig. 4 for lay-up (I). The Figs. 4a and 4b depict the flutter and divergence speed, respectively, versus fiber orientation angle $[\theta_{i,j}]$ for USW, FSW and BSW configuration.

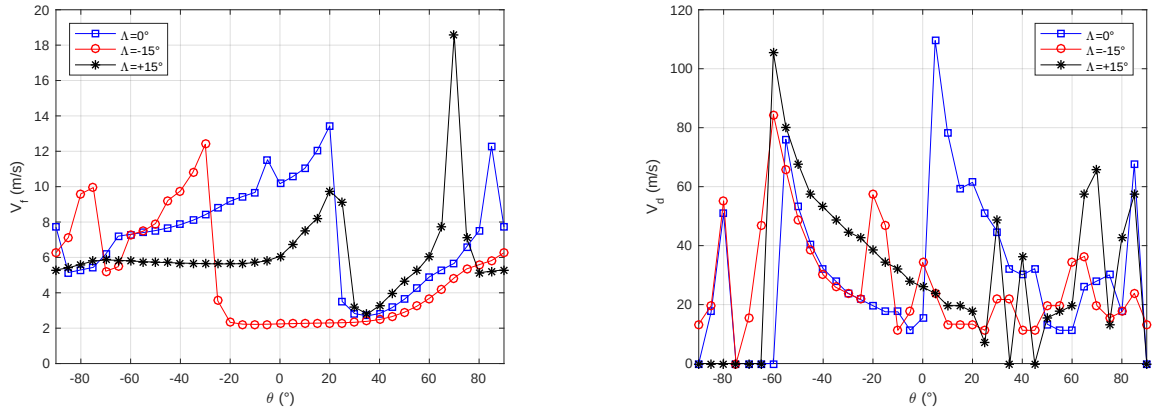

(a) Flutter speed results for lay-up (I) $[\theta_{1,1}]_S$ with 2 plies. (b) Divergence speed results for lay-up (I) $[\theta_{1,1}]_S$ with 2 plies.

Figure 4: Results of aeroelastic stability for lay-ups (I) and (II) with one fiber angle orientation variable.

The flutter and divergence behavior becomes more discontinuous when dealing with structures made of fiber reinforced composites. This happens because the change in fiber orientation angle reflects directly on modal analysis solution, changing modal shapes forms and frequencies, as well. The regions where fiber orientation is near $0°$ for USW, $-15°$ for FSW and $+15°$ for BSW present low resistance to first and second bending reflecting on low flutter speeds and divergence. The cases where divergence is equal zero in Fig. 4b mean that no divergence has been found in the speed range adopted in analysis. It is possible to find regions where both divergence and flutter speeds for FSW are equal or even higher than USW and BSW cases, for instance, when (I) is around $[-25°]_S$. Besides that, it is also important to note that small variations in lay-up orientation lead to very different flutter and divergence results.

Next, the mapping solutions for laminate (II) with two angles as variables are depicted with contour plots in Fig. 5. The Figs. 5a, 5b and 5c present flutter response for USW, FSW and BSW case, while Figs. 5d, 5e and 5f depict divergence speed behavior.

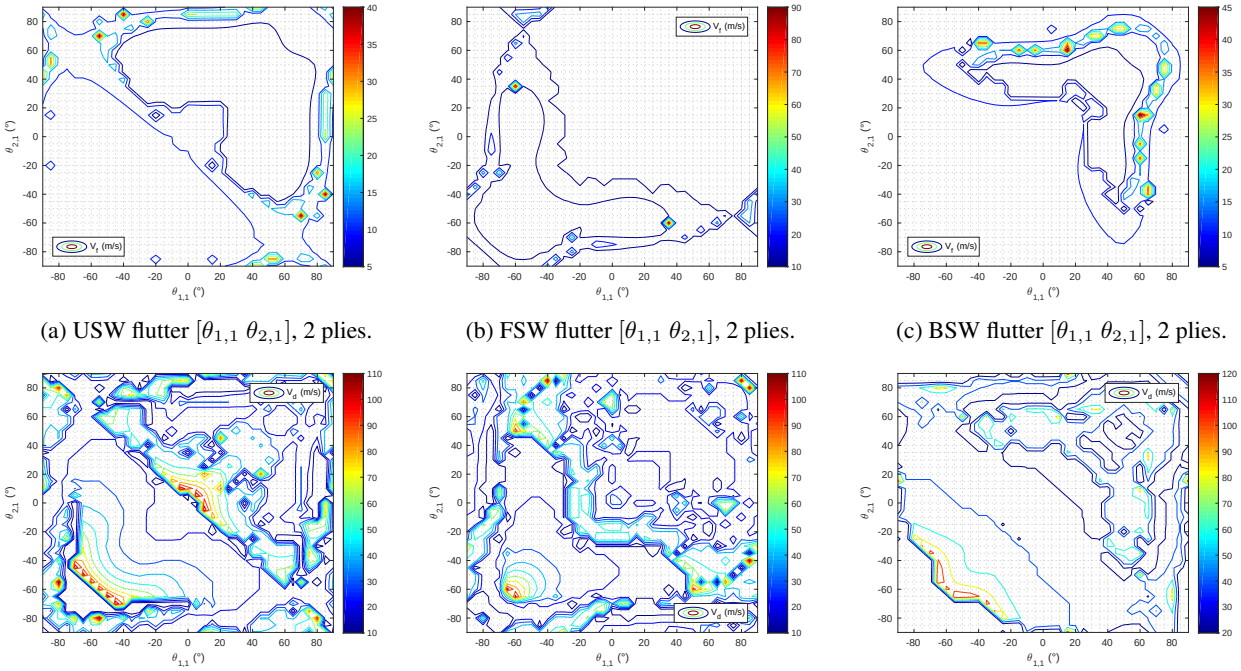

(a) USW flutter $[\theta_{1,1}\ \theta_{2,1}]$, 2 plies. (b) FSW flutter $[\theta_{1,1}\ \theta_{2,1}]$, 2 plies. (c) BSW flutter $[\theta_{1,1}\ \theta_{2,1}]$, 2 plies.

(d) USW divergence $[\theta_{1,1}\ \theta_{2,1}]$, 2 plies. (e) FSW divergence $[\theta_{1,1}\ \theta_{2,1}]$, 2 plies. (f) BSW divergence $[\theta_{1,1}\ \theta_{2,1}]$, 2 plies.

Figure 5: Contour plots presenting aeroelastic stability response of lay-up (II) $[\theta_{1,1}\ \theta_{2,1}]$ with 2 plies.

The lay-up (II) presents more complex results in relation to one variable case. The contour plots show that the aeroelastic tailoring technique may lay on very discontinuous solutions fields with many local minima and maxima. Thus, the direct employment of gradient-based optimization methods may not work properly in this case.

Therefore, heuristic or hybrid methods are suitable for application, such as GA or GA plus some gradient based method. Another fact demonstrated is that mapping technique is impracticable in systems with higher number of DGOF due the high computational time necessary to perform all possible cases. Thus, optimization must be employed to properly tailor the structure to the best aeroelastic response.

Based on that, the GA method has been adopted in this work by coupling ASA-T with Matlab® GA tool box. The lay-ups are optimized with initial population of 30 individuals genetically improved over 50 generations. The fiber orientation angles are considered integer numbers since it is not practicable to work with decimal angles when manufacturing laminates. The results are presented in Tab. 3. Besides that, the sign of composite stiffness matrix terms D_{16} and D_{26} are presented for optimized lay-ups in order to relate it with the wash-in and wash-out effect, as given in Shirk *et al.* (1986); Stanford *et al.* (2014). Negative values of both terms represent an counter wash-in effect, which may controls the FSW instability. Positive values represent an counter wash-out effect, which may control BSW instability. For D_{16} and D_{26} equal zero a symmetric bending without torsion-bending coupling is observed. The lay-up (I) with one DGOF does not present counter wash-in for FSW case, but only counter wash-out for BSW model. On the other hand, lay-up (II) with 2 DGOF can greatly represent counter bending-twisting coupling increasing flutter and divergence stabilities.

The results for asymmetric laminate presented values of flutter speed higher than symmetric case. This behavior occurs because the flutter couples the vibrational modes of bending and torsion. The ideal case for bending only will be all fibers orientated in span direction. On the other hand, for torsion only, fibers should be orientated at $\pm 45°$. Values near these best cases for isolated modes are found for lay-up (II) in each laminae. Even though, from the manufacturing point of view, asymmetric laminates suffer warping problem when cured, or in other words, $[\mathbf{B}] \neq [\mathbf{0}]$. Thus, it is believed that in

short future with the advance of manufacturing techniques for fiber reinforced composite laminates, the warping problem present in asymmetric lay-ups will be overcame making possible their utilization in composite aerospace structures.

Table 3: Optimized lay-ups with GA for maximum flutter speed.

Lay-up	Λ (°)	Opt. Lay-Up	V_f (m/s)	sign(D_{16})	sign(D_{26})
(I) $[\theta_{1,1}]_S$	0	$[86°]_S$	19.67	+	+
	-15	$[77°]_S$	15.35	+	+
	$+15$	$[70°]_S$	20.03	+	+
(II) $[\theta_{1,1}\ \theta_{2,1}]$	0	$[-48°\ 83°]$	48.86	-	-
	-15	$[-75°\ -37°]$	47.68	+	-
	$+15$	$[87°\ 39°]$	48.88	+	+

4. CONCLUSIONS

This work has proposed a methodology to aeroelastic tailor flexible swept wings made of fiber reinforced composite materials with constant stiffness. The formulation of aeroelastic models based on structure finite element implemented in DS Abaqus® and unsteady incremental aerodynamics with panel method implemented with Zaero® was briefly derived. The in house developed software ASA-T has been developed to automate the pre-process, run and pos-processing of these models. The tailoring is performed with genetic algorithm optimization method by using the Matlab® toolbox. In order to validate the aeroelastic stability function, an isotropic flexible wing made of aluminum with a ballast mass attached at its tip was modeled with three different sweep angles, $\Lambda = 0°$, $\Lambda = -15°$ and $\Lambda = +15°$ with tip chord remaining parallel to stream flow. The results of flutter for isotropic wing were validated with wind tunnel tests. The effect of ballast mass on aeroelastic stability was presented for each sweep configuration demonstrating the regions where the flutter may be overcome based on a desired flight envelope, characterizing also a kind of passive aeroelastic control in isotropic structures. It was demonstrated that forward swept wings made of aluminum present low divergence speeds that are increased by making the structure thicker and consequently expanding the structure weight. Moreover, wings with same geometry of isotropic but made of carbon-epoxy were investigated with two different lay-ups. The first lay-up has the same orientation angle for two plies, resuming an one degree of freedom optimization problem. The second lay-up has also two plies, but the fiber orientation angle may differ, resulting in an asymmetric lay-up with two degrees of freedom. The flutter and divergence speed of both lay-ups were mapped and optimized using GA optimization method. The results presented that composite structures can overcome the weight drawback issue by using aeroelastic tailoring techniques. With same mass, the optimized swept wings made of composite could increase flutter and divergence speeds. This work is being developed at ITA to deals with higher number of layers and variable stiffness laminates.

5. REFERENCES

Balvedi Junior, E.A., 2010. "Linear and nonlinear aeroelastic analyses of a typical airfoil section with control surface freeplay". *Master Thesis, Technological Institute of Aeronautics (ITA)*.

Bisplinghoff, R.L., Ashley, H. and Halfman, R.L., 2002. *Principles of Aeroelasticity*. Dover Inc., Mineola, New York.

Daniel, I.M., Ishai, O., Daniel, I.M. and Daniel, I., 2006. *Engineering mechanics of composite materials*, Vol. 2. Oxford university press New York.

Diederich, F.W. and Budiansky, B., 1948. *Divergence of swept wings*. National Advisory Committee for Aeronautics.

Diederich, F.W. and Foss, K.A., 1953. "Charts and approximate formulas for the estimation of aeroelastic effects on the loading of swept and unswept wings". *Report 1139, Langley Aeronautical Laboratory*.

Dillinger, J.K.S., Klimmek, T., Abdalla, M.M. and Gürdal, Z., 2013. "Stiffness Optimization of Composite Wings with Aeroelastic Constraints". *Journal of Aircraft*, Vol. 50, No. 4, pp. 1159–1168. ISSN 0021-8669. doi: 10.2514/1.C032084.

Försching, H.W., 2013. *Grundlagen der aeroelastik*. Springer-Verlag.

Fung, Y.C., 2002. *An introduction to the theory of aeroelasticity*. Courier Corporation.

Gudmundsson, S., 2013. *General aviation aircraft design: Applied Methods and Procedures*. Butterworth-Heinemann.

Harder, R.L. and Desmarais, R.N., 1972. "Interpolation using surface splines." *Journal of aircraft*, Vol. 9, No. 2, pp. 189–191.

Hertz, T.J. and Picchioni, F.A., 1981. "Aeroelastic Tailoring with Composites Applied to Forward Swept Wings". *Nasa Langley Report AFWAL-TR-81-3043*.

Inc., M., 2017. "Matlab r2017a - optimization toolbox user's guide". *The MatWorks Inc*.

Jaworski, J.W., 2009. "Nonlinear aeroelastic analysis of flexible high aspect ratio wings including correlation with experiment". *PhD Thesis, Graduate School of Duke University*.

Kameyama, M. and Fukunaga, H., 2007. "Optimum design of composite plate wings for aeroelastic characteristics using lamination parameters". *Computers & structures*, Vol. 85, No. 3, pp. 213–224.

Krone, JR, N., 1980. "Forward swept wing flight demonstrator". In *Aircraft Systems Meeting*. p. 1882.

Krone, N.K.J., 1975. "Divergence Elimination with Advanced Composites". *AIAA Journal*, Vol. 1009. doi: 10.2514/6.1975-1009.

Krüger, W.R., Klimmek, T., Liepelt, R., Schmidt, H., Waitz, S. and Cumnuantip, S., 2014. "Design and aeroelastic assessment of a forward-swept wing aircraft". *CEAS Aeronautical Journal*, Vol. 5, No. 4, pp. 419–433.

Lanczos, C., 1950. "An iteration method for the solution of the eigenvalue problem of linear differential and integral operators". *Research paper 2133. Journal of Research of the National Bureau of Standards*, Vol. 45, No. 4.

Liu, D., Toropov, V.V., Barton, D.C. and Querin, O.M., 2015. "Weight and mechanical performance optimization of blended composite wing panels using lamination parameters". *Structural and Multidisciplinary Optimization*, Vol. 52, No. 3, pp. 549–562.

Piening, M., 1984. *Die statische Aeroelastizität des anisotropen Tragflügels: Vortrag 84-158; DGLR-Symposium Entwicklung und Anwendung von CFK-Strukturen, Technische Universität Berlin, 8. und 9. November 1984*. DFVLR.

Reddy, J.N., 2004. *Mechanics of laminated composite plates and shells: theory and analysis*. CRC press.

Reddy, J.N., 2005. *An introduction to the finite element method*, Vol. 3. McGraw-Hill New York.

Redeker, G. and Wichmann, G., 1991. "Forward Sweep — A Favorable Concept for a Laminar Flow Wing". *AIAA Journal*, Vol. 28, No. 2.

Ricketts, R.H. and Doggett Jr, R.V., 1980. "Wind-tunnel experiments on divergence of forward-swept wings".

Roldo, G., 2016. "Um estudo sobre otimização aeroelástica usando compósitos laminados de rigidez variável na maximização da velocidade de flutter". *Graduation Work. Federal University of Rio Grande do Sul, Porto Alegre, Brazil.*

Shirk, M.H., Hertz, T.J. and Weisshaar, T.A., 1986. "Aeroelastic tailoring-theory, practice, and promise". *Journal of Aircraft*, Vol. 23, No. 1, pp. 6–18.

Shokrieh, M.M. and Lessard, L.B., 2000. "Progressive fatigue damage modeling of composite materials, part i: Modeling". *Journal of Composite Materials*, Vol. 34, No. 13, pp. 1056–1080.

Stanford, B.K. and Jutte, C.V., 2014. "Aeroelastic tailoring via steered composites". *NASA Langley Research Center TM–2014-218517*.

Stanford, B.K., Jutte, C.V. and Wu, K.C., 2014. "Aeroelastic benefits of tow steering for composite plates". *Composite Structures*, Vol. 118, pp. 416–422.

Thuwis, G.A., De Breuker, R., Abdalla, M.M. and Gürdal, Z., 2010. "Aeroelastic tailoring using lamination parameters". *Structural and Multidisciplinary Optimization*, Vol. 41, No. 4, pp. 637–646.

Tian, W., Yang, Z., Gu, Y. and Ouyang, Y., 2016. "Aeroelastic tailoring of a composite forward-swept wing using a novel hybrid pattern search method". *Journal of Aerospace Engineering*, Vol. 29, No. 6, p. 04016056.

Tsai, S.W., 1966. "Mechanics of composite materials". *AFML-TR-66-149, Air Force Materials Laboratory, Wright-Patterson AFB*.

Uranga, A., Persson, P.O., Drela, M. and Peraire, J., 2011. "Preliminary investigation into the effects of cross-flow on low reynolds number transition". In *20th AIAA Computational Fluid Dynamics Conference*. p. 3558.

Waddoups, M., McCullers, L. and Naberhaus, J., 1971. "Composite wing for transonic improvement". Technical report, AFFDL-TR-71-24, Nov.

Weisshaar, T., 1995. "Aircraft aeroelastic design and analysis". *School of Astronautics and Aeronautics-Purdue University, Class Notes*.

Weisshaar, T.A., 1978. "Aeroelastic stability and performance characteristics of aircraft with advanced composite swept-forward wing structures". *AFFDL-TR-78-116*.

Weisshaar, T.A., 1979. "Forward Swept Wing Static Aeroelasticity". *Virginia Polytechnic Institute and State University. AFFOL-TR-79-3087*.

Weisshaar, T.A., 1980. "Divergence of Forward Swept Composite Wings". *AIAA Journal*, Vol. 17, No. 6, pp. 442–448.

Weisshaar, T.A., 1981. "Aeroelastic Tailoring of Forward Swept Composite Wings". *AIAA Journal*, Vol. 18, No. 8, pp. 669–676.

Werter, N.P., Sodja, J. and De Breuker, R., 2016. "Design and testing of aeroelastically tailored wings under maneuver loading". *AIAA Journal*, pp. 1–14.

Whitford, R., 1987. *Design for air combat*. 1st edition. Janes Information Group.

ZONA-Technology, 2009. "Zaero theoretical manual". *ZONA Technology Inc., 15a edn. 9489 E. Ironwood Square Drive, Scottsdale,Arizona, USA*.

6. RESPONSIBILITY NOTICE

The authors are the only responsible for the printed material included in this paper.